

# Melt Processability of Polytetrafluoroethylene: Effect of Melt Treatment on Tensile Deformation Mechanism

Min Li,<sup>1</sup> Wei Zhang,<sup>2</sup> Chaosheng Wang,<sup>1</sup> Huaping Wang<sup>1</sup>

<sup>1</sup>College of Materials Science and Engineering, Donghua University, Shanghai 201620, China

<sup>2</sup>School of Polymer Textile and Fiber Engineering, Georgia Institute of Technology, Atlanta, Georgia 30332

Received 18 January 2011; accepted 1 April 2011

DOI 10.1002/app.34625

Published online 19 August 2011 in Wiley Online Library (wileyonlinelibrary.com).

**ABSTRACT:** It is widely accepted that the melt processability of polytetrafluoroethylene (PTFE) is poor. In this article, a high-molecular-weight PTFE was extruded smoothly with a modified die; and critical shear rate could be raised to  $4 \text{ s}^{-1}$ , using a die with  $L/D$  (length to diameter) ratio of 200. Meanwhile, we compared the current PTFE fiber spinning method with melt spinning to investigate the effects of high-temperature treatment on the drawability of PTFE and found that the processing sequence could play a key role. The deformation imposed before or after the high-temperature treatment could determine whether the fibrillation can

be achieved continuously and effectively. Based on the experiment phenomenon, together with the results of differential scanning calorimetry, X-ray diffraction, and scanning electron microscopy characterization, we proposed a model to describe the submicron structural change of PTFE during extension. From this model, the fundamental mechanism for the poor melt processability of PTFE was elucidated. © 2011 Wiley Periodicals, Inc. *J Appl Polym Sci* 123: 1667–1674, 2012

**Key words:** polytetrafluoroethylene; melt; processability; extrusion; entanglement; drawability

## INTRODUCTION

Because of its extreme chemical inertness, thermal stability, and many other desirable physical properties, polytetrafluoroethylene (PTFE) has been widely used in applications, where the material needs to be imposed under extreme serving conditions.<sup>1–3</sup> Usually high-molecular-weight PTFE is classified as non-melt processable, because of its high-melt viscosity.<sup>4</sup> Conventional processing technique for converting PTFE into fibers involves multiple steps, such as formation of kerosene/PTFE paste followed by stretching and sintering<sup>5–7</sup> or creation of PTFE/matrix polymer emulsion followed by emulsion spinning and sintering.<sup>8,9</sup> Because these processes involve the usage of large amount of solvent or decomposition of emulsion matrix, it is highly desired to develop a technique capable of processing PTFE fiber in a simple and environment friendly manner. Recently, Badding and coworkers<sup>10</sup> tried jet blow high-molecular-weight PTFE both above and below its melting point. In this method, a two phase mixture of PTFE and gas was driven by pressure through a single spinneret and sequentially split into multiple thin fibers near the spinneret. But their method could

only produce mat of millimeter long micro/nanofibrous; it cannot be used to create continuous filament. Tervoort et al. developed melt-processable PTFE for generating continuous fiber.<sup>4,11</sup> They blended high-molecular-weight (intractable) PTFE with low molecular weight one or introduced perfluoro-propylvinylether into the backbone of the fluoropolymer. Though continuous filament was generated using this technique, these modifications were found to damage the desired properties of pure high-molecular-weight PTFE.

On the other hand, ram extrusion is often considered to be a proper choice for processing high-molecular-weight and consequently high-viscosity polymer.<sup>12</sup> High viscosity and obvious elasticity of PTFE make it unsuitable to be processed by screw extruder. However, a ram extruder with sufficient power can be applied successfully to extrude PTFE, because the surface energy of the PTFE is low and slippage at the extrudate/die interface can easily happen. As unnecessary shear during flow can be greatly reduced by the aforementioned wall slippage, the required pressure is not unreachable high. Because of this, ram extrusion was thought to be a promising approach for melt processing of high-molecular-weight PTFE. Unfortunately, the critical shear rate of PTFE is of the order of  $10^{-5} \text{ s}^{-1}$ , which is unreasonable for real world industrial application.<sup>13</sup> In this article, this parameter was increased to a much feasible value, and stable extrusion of PTFE was realized by modifying the die design.

Correspondence to: C. Wang (cswang@dhu.edu.cn).

Contract grant sponsors: Fundament Research Funds for the Central Univesity, 2009; China Scholarship Council.

Though the extrusion instability was successfully overcome, the lack of melt strength was noticed by the authors. After molten PTFE formed a neck under tensile force, the material did not show the needed strain hardening effect so that the necking region could be stabilized. Instead, the extrudate broke at the necking region, and the spinning process stopped. Actually, similar descriptions have been reported by several researchers as well.<sup>10</sup> However, the mechanism for the cause of these difficulties encountered in melt spinning of PTFE has not been touched. In this study, authors compared the current PTFE spinning methods with normal melt spinning process and found that the processing sequence took a key role in spinning PTFE. The deformation imposed before or after the high-temperature treatment could determine whether the fibrillation can be achieved continuously and effectively. Experiments were conducted to understand the structural changes of PTFE after the melting treatment and changes of material drawability.

## EXPERIMENTAL

### Materials

PTFE powder was acquired from Chenguang Research Institute of Chemical Industry (Sichuan). The average particle size is around 250 nm, Figure 1. According to the model provided by Suwa<sup>14</sup>:

$$\overline{M}_n = 2.1 \times 10^{10} \Delta H_c^{-5.16}$$

$\overline{M}_n$  is the number average molecular weight,  $\Delta H_c$  is the fusion of crystalline ( $\text{cal g}^{-1}$ ), and the calculated molecular weight is  $1.03 \times 10^9 \text{ g mol}^{-1}$ .

The lubricant used in the experiment is kerosene, which has a boiling point of 150–280°C, flash point of 43–72°C, and density of  $0.9 \text{ g cm}^{-3}$ .

### Preparation

PTFE was extruded using ram extruder in two ways, including melt extrusion and paste extrusion. Melt extrusion was performed in one step by extruding the melted PTFE at 380°C through single capillary orifice. The applied pressure was around 89 MPa. Three dies were used: Die 1 ( $L/D = 1$ ), Die 2 ( $L/D = 20$ ), and Die 3 ( $L/D = 200$ ), the diameter is 0.5 mm for all dies.

Paste extrusion was carried out on the same machine. First, PTFE powder was lubricated with kerosene. The resulting paste of 85 wt % PTFE was then aged at room temperature in an airtight container for 12 h to allow a uniform wetting. Following this, the paste was then extruded at room temperature through Die 2.

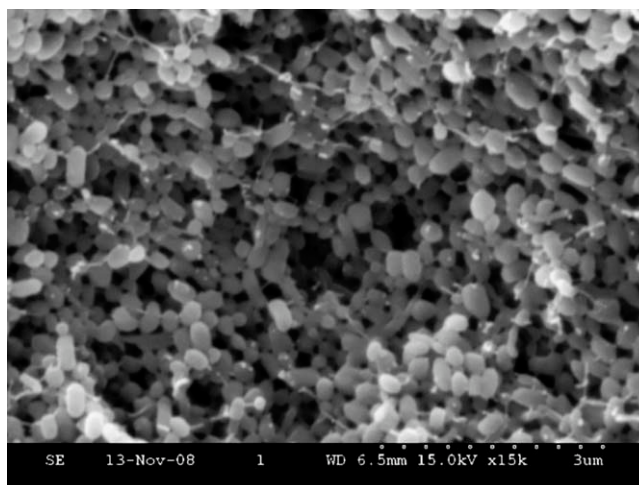


**Figure 1** Original PTFE particle morphology: the particle size is about 250 nm.

The extrudate was baked at 120°C for 12 h to remove the kerosene. The baked extrudate was later compressed into film with a pressure of 40 MPa at room temperature. Some of these films were melted at 380°C for 5 min then cooled down in the air. In the extension test, both these raw compressed films and melted films were stretched at 270°C with Instron at a rate of  $10 \text{ mm min}^{-1}$ . The drawing ratio was calculated through measuring the change of the distance between two marked points on the sample before and after extension.

### Characterization

Various characterization techniques, including differential scanning calorimetry (DSC), X-ray diffraction (XRD), and scanning electron microscopy (SEM), were used to investigate the structure and morphology of materials produced in this study. DSC (TA Q200) analysis was performed at a heating rate of  $10^\circ\text{C min}^{-1}$ . For XRD, disks made of gently compressed PTFE powder were directly inspected on X'Pert PRO Alpha-1. SEM (LEO SEM 1550 at 5 kV) was used to examine the fibrous structure after stretching. The SEM samples were sputtered with a gold/platinum alloy prior to SEM observation. Dynamic mechanical analysis (DMA) (TA Q800) test was conducted in a temperature range from room temperature to 270°C at a ramping rate of  $5^\circ\text{C min}^{-1}$ , with frequency of 1 Hz.

## RESULTS AND DISCUSSION

Melt extrusion of PTFE was performed in a single step by extruding the high-viscous polymer through an orifice continuously. We used three different dies with  $L/D$  ratios of 1, 20, and 200. Scanning electron microscope images (Fig. 2) demonstrate the surface

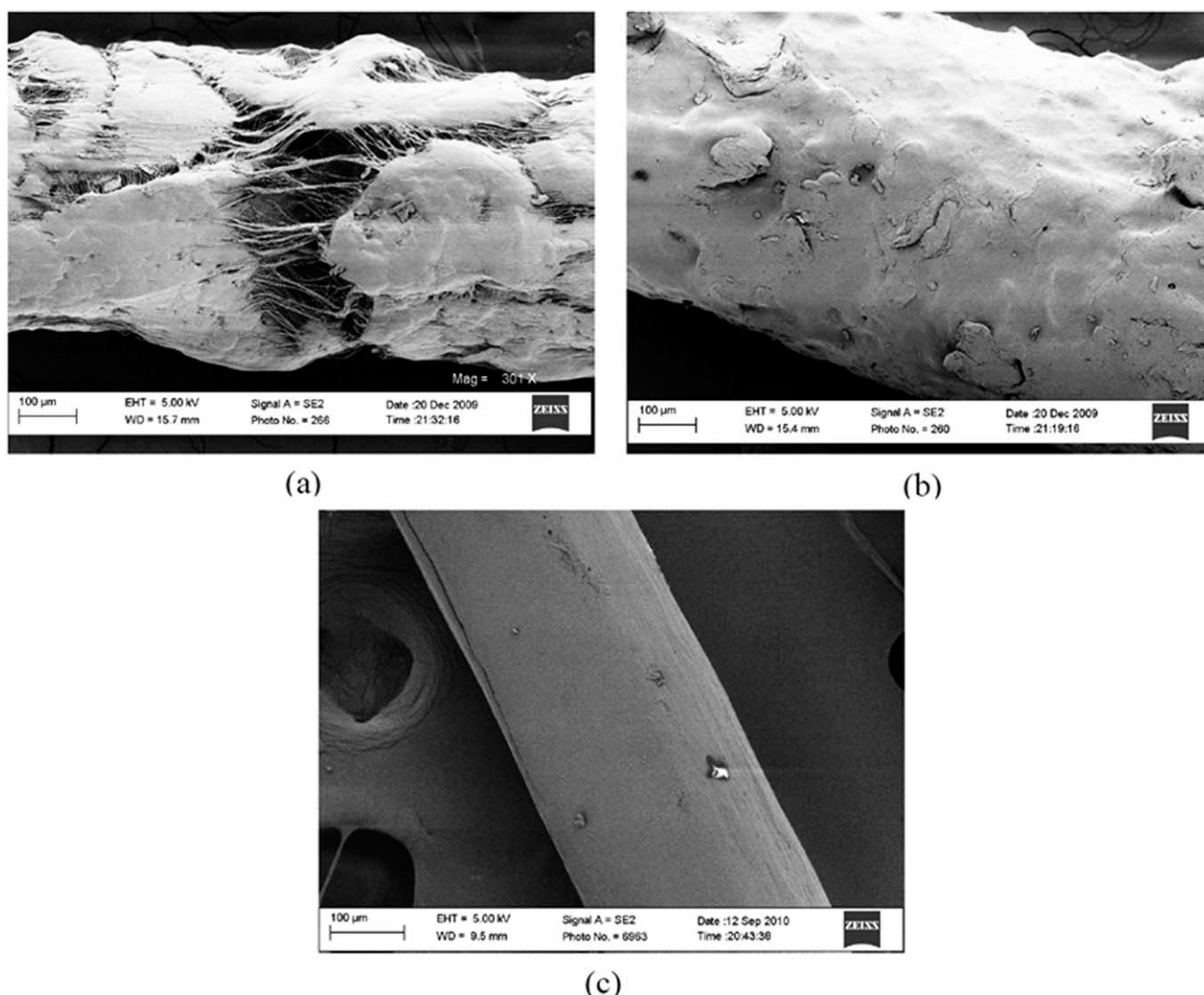


**Figure 2** Surface morphology of melt PTFE extrudate with different dies: (a) Die 1; (b) Die 2; and (c) Die 3.

morphology of PTFE extrudate from different dies. Before coming to the orifice, the PTFE melt flow under pressure in a tube with a diameter of 12 mm. Strong extensions and shear were applied on the melt flow near the entrance of the capillary, where sudden abrupt contraction happens. On one hand, the combinational effect of extensile and shear forces greatly enhanced the orientation and fibrillation of the PTFE. Additionally, the abrupt contraction induced extra elasticity to the highly viscous PTFE melt. The jagged surface of the extrudate from Die 1 [Fig. 2(a)] suggests the elastic instability. However, it should be noted that the surface became smoother when die with larger  $L/D$  ratio was used. No obvious break or jag could be found on the surface of extrudate from Die 2. When the  $L/D$  ratio was increased to 200, a much smoother surface was achieved as in Figure 2(c). In all the extrusion experiment, the head speed was kept the same, which gave an approximate shear rate of  $4 \text{ s}^{-1}$ . Compared with previously reported critical shear

rate of  $10^{-5} \text{ s}^{-1}$ , this value was drastically increased by utilizing die with large  $L/D$  ratio. The main reason for this large improvement was that the higher  $L/D$  ratio could suppress the unwanted elastic instability. Although die with large  $L/D$  ratio was able to reduce the negative influence from melt elasticity, it was also found that the melt strength of PTFE was too low to be drawn into continuous fiber. Actually, after molten PTFE formed a neck under tensile force, the material did not show the needed strain hardening effect, so that the necking region could be stabilized. Instead, the extrudate broke at the necking region, and the spinning process stopped.

Through comparing the current PTFE fiber spinning method with the melt spinning method, it was found that the processing sequence plays a key role in the successfully spinning PTFE. For current industrial practice, there are two main methods to produce PTFE fiber, namely, expanded PTFE spinning and matrix spun PTFE. In the expanded PTFE spinning method, PTFE/kerosene paste was first



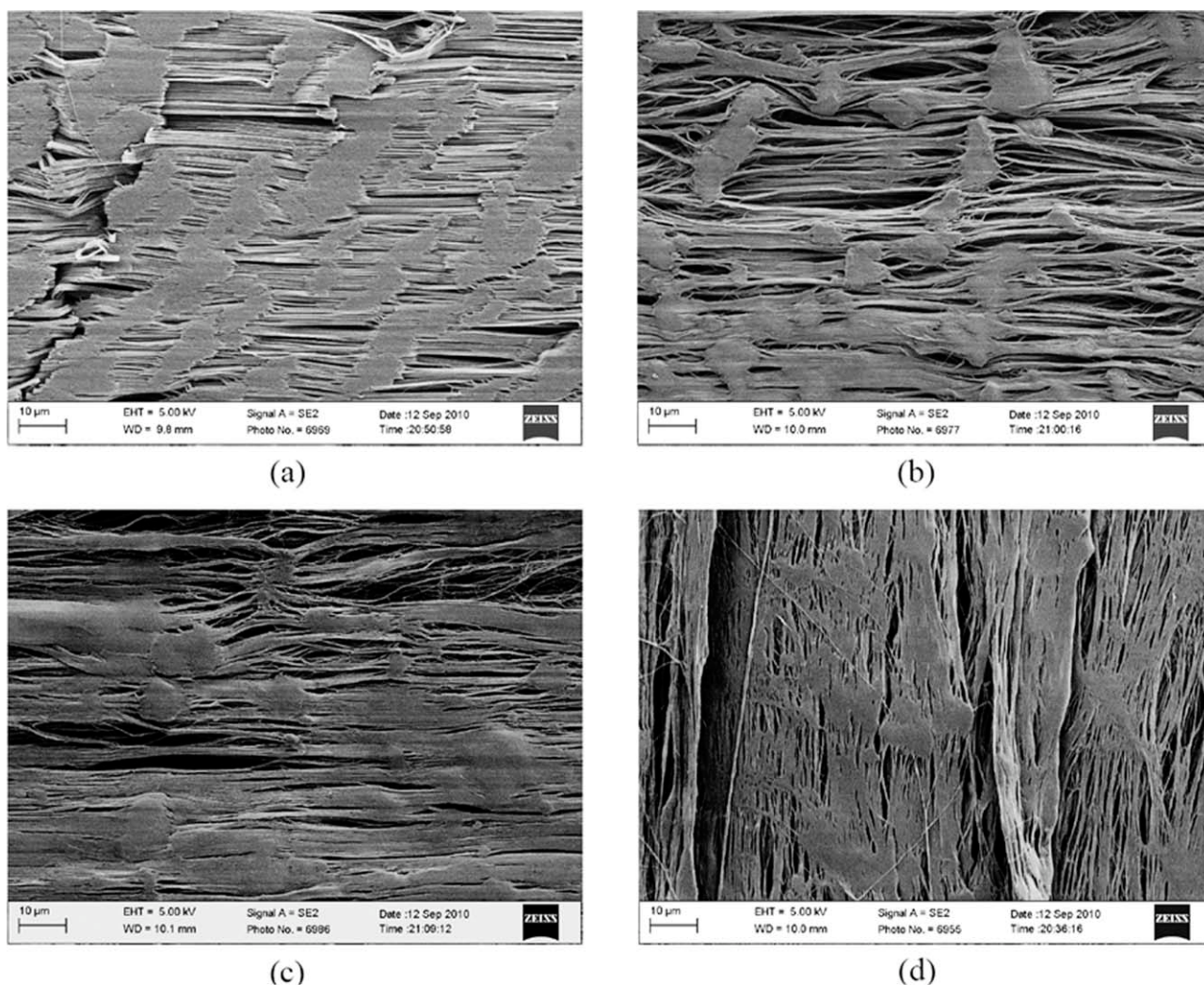


**Figure 3** Raw PTFE film extended different ratios at 270°C: (a) three times; (b) 10 times; (c) 20 times; and (d) 30 times.

extruded by a ram extruder. Later, the extruded rod was compressed and stretched at 270°C, which was lower than the melting temperature of PTFE. The obtained sample was further stretched to the final diameter at a temperature above its melting point. In the case of matrix spinning method, PTFE aqueous dispersion was mixed with a solution of a suitable matrix polymer, the initial mixture was turned into an intermediate filament, after it went through a coagulation bath.<sup>15</sup> The intermediate filament was quickly heated to a high temperature to decompose the matrix polymer and form a brown color PTFE fiber. For both methods, PTFE was initially deformed and fiberized at a temperature much below the melting temperature. The produced filament was further treated at a higher temperature either above the PTFE melting point or the degradation temperature of the matrix polymer. Through this type of two-stage thermal treatment, both methods were able to cleverly bypass the issue of low melt strength encountered in our previous

one-step melt spinning experiment and create PTFE fibers.

Figure 3 shows the submicron morphology of PTFE raw film after a low temperature drawing. It could be seen that with an increase of extension ratio, the fiber become finer and finer. In this case, the initial film could be elongated more than 30 times at 270°C. However, the melted film could only be stretched to a maximum ratio of 3. Because the drawing ration was low for the melt drawing case, no obvious fibril formation was found, Figure 4. In the experiment, it was found that the raw PTFE powder changed from sticky and soft into nonsticky and rigid after a melting-cooling cycle. In other words, the raw PTFE powder is easier to be deformed into fiber, but after the melt treatment, it is more inclined to maintain original state. This also could be reflected from the local morphology of the broken end, in Figure 5, where the raw PTFE material shows some long microfiber, but the melted film only has some short microfiber.

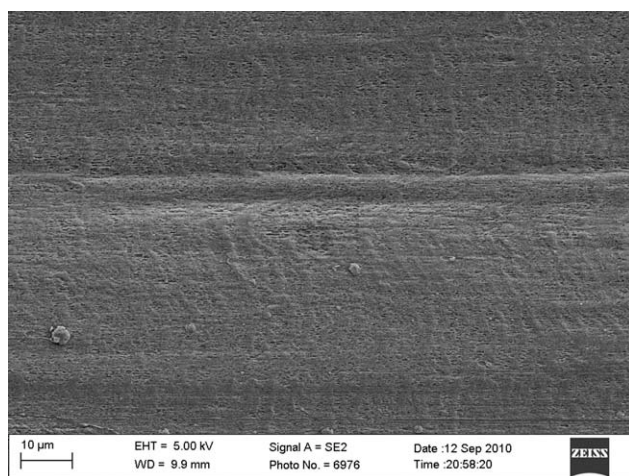


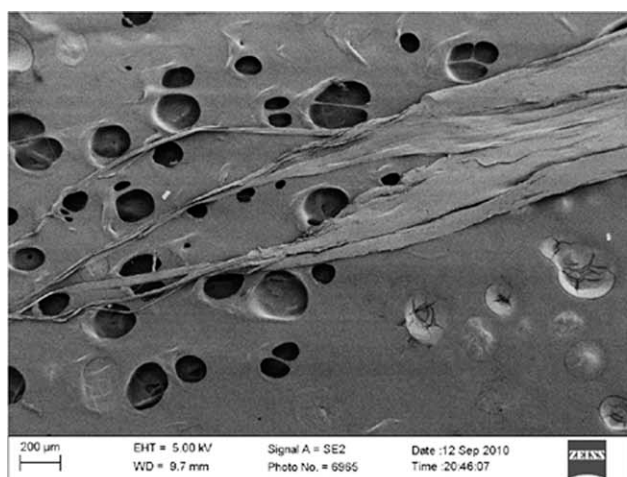
**Figure 4** Melted PTFE film extended three times at 270°C.

To verify whether the change of material property was originated from removal of residual surfactant in polymerization, original PTFE powder was heated to 380°C in gas chromatography–mass spectrometer to detect the small molecular. But no trace of volatile was found. In addition, there was no measurable decrease of weight at the thermo-gravimetric analysis until 480°C, which was because of decomposition of PTFE polymer, shown in Figure 6. The signal of any small molecule coated on the PTFE powder was not detected in solid NMR. FTIR-ATR spectra of compressed and melted PTFE film are shown in Figure 7. The typical fluorocarbon spectrum associated with stretch vibration  $\text{CF}_2$  is 1100–1300  $\text{cm}^{-1}$ .<sup>16,17</sup> No new peak appears after the film go through high-temperature sintering, which means that high-temperature treatment does not lead to new chemical bond. Therefore, it can be naturally presumed that the rea-

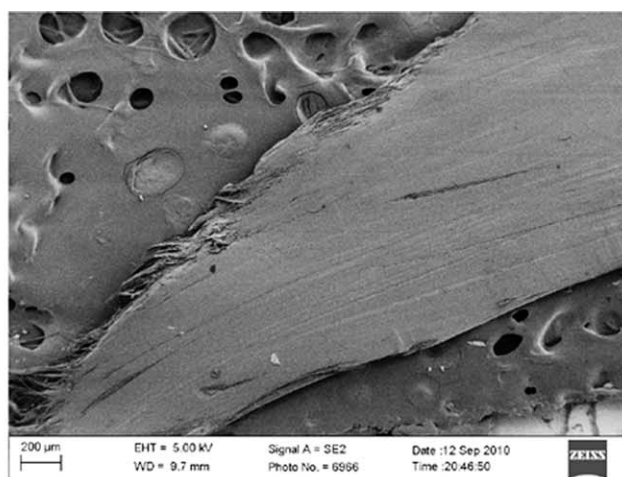
son for property change is that the melt treatment alters the PTFE supramolecular structure.

It was well documented that supramolecular structure related closely with material property. Two requirements for the ultradrawability include mobility of chains, and a low degree of entanglement which is important for the stress transfer. The peculiar PTFE helical structure imposes the chain high mobility, and chains can move through and out of the crystals easily.<sup>18</sup> In the raw PTFE film, the sticky nanoparticles are easy to aggregate closely, and the adhesion force among the particles can provide sufficient “entanglement.” Because the particle is soft, they would be stretched thinner before they are separated during drawing. The situation for the film after melt treatment is just on the contrary. The chain movement in rigid particle is relative more difficult, and the stress could not be transferred effectively because of the lack of adhesion among the nonsticky particles. As the property change does not result from removal of surfactant or altered chemical structure, it is reasonable to suppose that melt induces irreversible transformation of PTFE supramolecular structure.

Actually, the unrecoverable crystalline of high-molecular-weight PTFE after a melting–cooling cycle has been reported by previous literature.<sup>19</sup> The raw PTFE powder which crystallizes from solution during polymerization tends to form extended chain with folded ribbons and has perfect crystal.<sup>20–23</sup> Thermal analysis and crystalline test, presented in Figure 8, shows that raw PTFE has higher melting enthalpy and a sharp crystallization peak. After the melting–cooling cycle, the melting point of PTFE becomes lower; the peak in XRD is not sharp anymore, and a shoulder peak appears around 15° which is attributed to amorphous region.<sup>24,25</sup> This is



(a)



(b)

**Figure 5** Local morphology of breaking end of PTFE film drawn at 270°C: (a) raw film and (b) melted film.



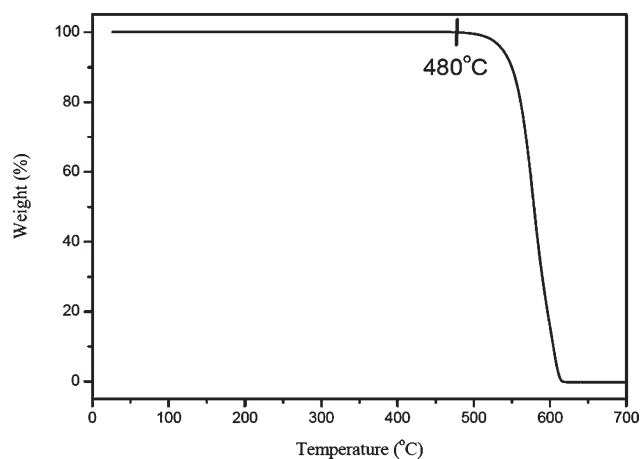


**Figure 6** Thermo-gravimetric curve of PTFE powder.

because when the temperature is above the melting point of PTFE, the polymer chain will become amorphous and get entangled with each other. For high-molecular-weight PTFE, once the macromolecules melt and entangle with each other they cannot restore to high crystallinity.<sup>26</sup> And the entanglement also plays the role of physical crosslinking. It is well known that with the increase of crosslink and entanglement density, impact strength of the material will be enhanced and the ductility will be diminished.<sup>27</sup> This is consistent with hardening of PTFE after melt treatment.

The viscoelastic and relaxation characteristics could well illustrate the supramolecular structural change of material. The result of DMA is presented in Figure 9. The dynamic storage modulus ( $E'$ ) and loss  $\tan \delta$  factor of raw film and melted film are plotted as a function of temperature. It can be observed that storage modulus of melted film is higher than the raw

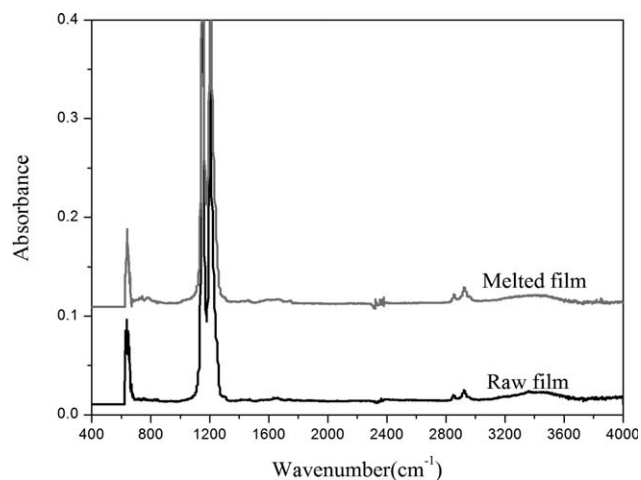


**Figure 7** FTIR-ATR spectrum of raw and melted PTFE film.

film in the low temperature range. This means the elasticity of the melted film is more obvious, and the melted film is more likely to keep original state. With the increase of temperature, storage modulus of both films decreases, as the mobility of chain segment is enhanced. After the temperature exceeds 140°C, storage modulus of melted film declines faster than that of the compressed film. It indicates that connection among the particles begins to play a leading role controlling mechanical response at elevated temperature. This may result from the weak points among particles. As the PTFE particle is polyhedral, the PTFE chains can be perpendicular or parallel to the faces. And the neighboring particles can coalesce into each other only when two like faces which contain ends come into contact.<sup>12</sup> Weak point can be formed at the contact between the unlike faces. As the particle becomes rigid, it is much harder for deformation.

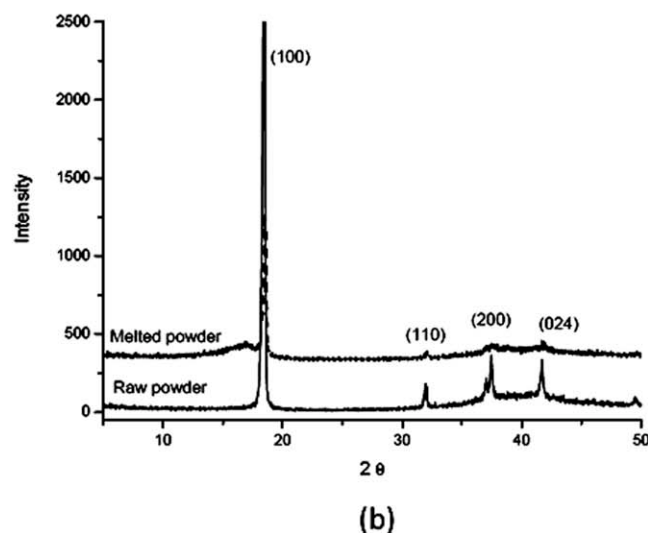
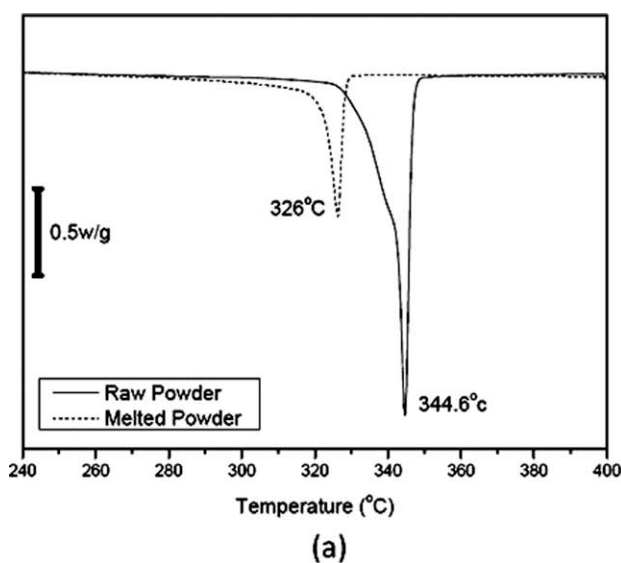


**Figure 8** DSC (a) and XRD (b) test before and after melt.

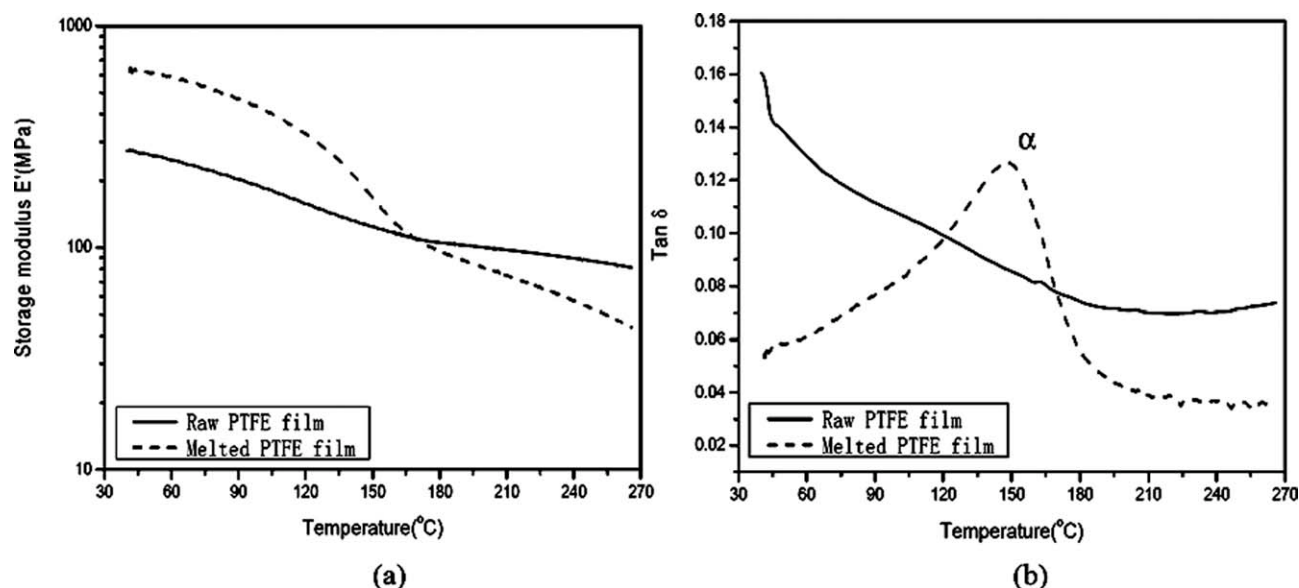


Figure 9 DMA test of PTFE film before and after melt: (a) storage modulus and (b)  $\tan \delta$ .

When the stress is larger, these weak points will be the stress concentration point leading to the breakage. After the temperature rises higher than 160°C, the storage modulus of melted film is smaller than that of raw PTFE film.

On the curves of loss  $\tan \delta$  factor versus temperature, Figure 9(b), a peak can be observed at about 150°C for the melted PTFE, which is attributed to be  $\alpha$  transition resulted from transition of amorphous PTFE chain.<sup>28–30</sup> It is widely agreed by the literature that the crystalline PTFE has broad glass transition temperature from  $-100$  to  $-50^\circ\text{C}$ ,<sup>29,31,32</sup> because local chain mobility is unhindered. The high transition temperature of the amorphous chain can be related to reduced mobility of macromolecular chains in the entanglement. This also can be reflected by the phenomenon that orientation happens more easily for the crystalline than for the amorphous PTFE chain. It has been documented that the crystallites of semicrystalline PTFE obtains a

high degree of alignment under uniaxial elongation, however, the amorphous chains keep an isotropic conformation.<sup>33</sup> In other words, the network structure between restricted amorphous PTFE chains largely suppresses the orientation of the molecules from the molten state.

Based on the experiment phenomenon, we propose the model for submicron structure change of PTFE during extension as shown in Figure 10. To some degree, whether PTFE can be elongated into fiber depends on the competition between the deformation capability of particles and boundary strength. For the raw PTFE film, the stress to deform the particle is much smaller than the cohesion among particles, so it can be elongated into long and continuous fibrous structure. But for the melted film, the particle boundary weak point breaks before the force applied on the film increases enough to elongate the hard particle into fiber, and some short fiber would be drawn out.

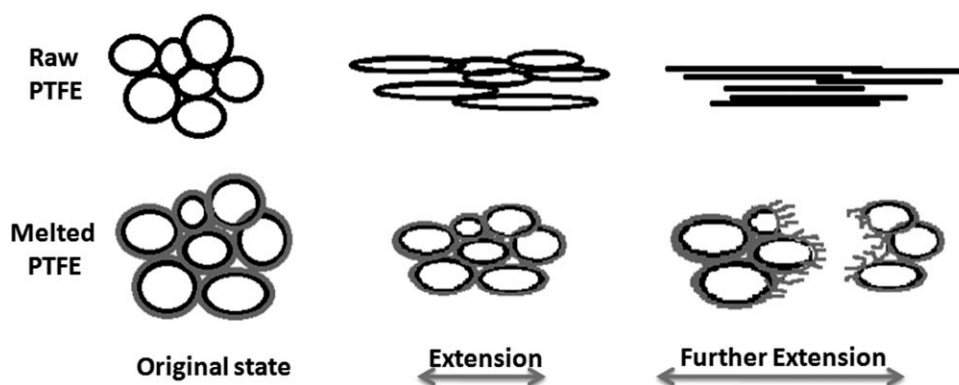
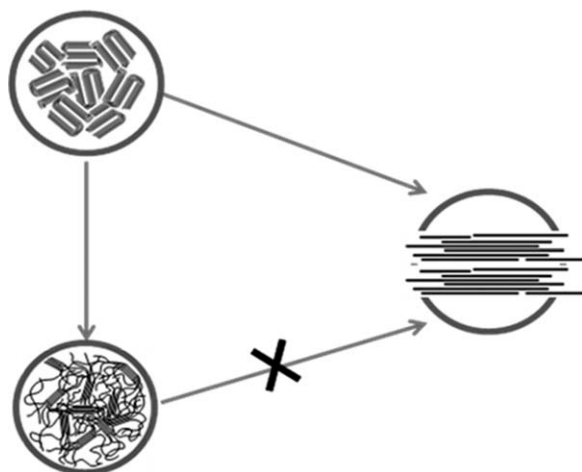


Figure 10 Model of PTFE film submicron structure change during extension.



**Figure 11** Scheme of PTFE structure transition.

Figure 11 depicts the structure transition of PTFE molecules. During the drawing, raw PTFE deforms in a ductile manner. Thus, the fibrillation of PTFE during the expanded spinning and matrix spinning can be carried out smoothly. However, once the raw PTFE go through melt, the intermolecular chain entanglement will form. To some extent, the entanglement acts as crosslink point and makes the material hard. It is the entanglement which restricts the molecular motion and makes it impossible to stretch orientated. This is the major reason why PTFE cannot be melt spun.

### CONCLUSIONS

We have observed that it is possible to extrude high-molecular-weight PTFE smoothly at relative high shear rate through die with larger  $L/D$  ratio. The critical shear rate can be raised to  $4 \text{ s}^{-1}$ , using the die with  $L/D$  of 200, and the elastic instability can be eliminated to the lowest degree. However, it is still impossible to directly melt spin PTFE fiber because of the low melt strength. Melt treatment makes the ductibility of raw PTFE disappear; melted PTFE is hard and difficult to deform. Tests show that the change is due to the supramolecular structure alteration. Entanglement of the melted PTFE works like crosslink points and would restrict the molecular motion. On one hand, it makes the material become

hard. On the other hand, it prevents chains from being stretched orientated.

### References

1. Rozen, S.; Menahem, Y. *J Fluor Chem* 1980, 16, 19.
2. Gangal, S. V. *Perfluorinated Polymers*; John Wiley & Sons, Inc.: New York, 2000.
3. O'Hagan, D.; Harper, D. B. *J Fluor Chem* 1999, 100, 127.
4. Tervoort, T.; Visjager, J.; Graf, B.; Smith, P. *Macromolecules* 2000, 33, 6460.
5. Nakajima, N.; Stark, C. F.; Kim, Y. J. *Trans Soc Rheol* 1972, 16, 761.
6. Ariawan, A. B.; Ebnesajjad, S.; Hatzikiriakos, S. G. *Polym Eng Sci* 2002, 42, 1247.
7. Ochoa, I.; Hatzikiriakos, S. G. *Powder Technol* 2005, 153, 108.
8. Xiong, J.; Huo, P. F.; Ko, F. K. *J Mater Res* 2009, 24, 2755.
9. Koldobskii, A. L.; Dreizenshtok, G. S.; Sorokin, E. Y.; Perepelkin, K. E.; Sliřko, L. V. *Fibre Chem* 1984, 15, 438.
10. Borkar, S.; Gu, B.; Dirmyer, M.; Delicado, R.; Sen, A.; Jackson, B. R.; Badding, J. V. *Polymer* 2006, 47, 8337.
11. Tervoort, T. A.; Visjager, J. F.; Smith, P. *J Fluor Chem* 2002, 114, 133.
12. Durrschmidt, T.; Hoffmann, H. *J Appl Polym Sci* 2004, 92, 733.
13. Tordella, J. P. *Trans Soc Rheol* 1963, 7, 231.
14. Suwa, T.; Takehisa, M.; Machi, S. *J Appl Polym Sci* 1973, 17, 3253.
15. Jones, C. W. U.S. Pat. 7,347,960, 2004.
16. Dannetun, P.; Schott, M.; Vilar, M. R. *Thin Solid Films* 1996, 286, 321.
17. Fischer, D.; Lappan, U.; Hopfe, I.; Eichhorn, K. J.; Lunkwitz, K. *Polymer* 1998, 39, 573.
18. Hu, W. G.; Schmidt-Rohr, K. *Acta Polym* 1999, 50, 271.
19. Radusch, H. J. *J Therm Anal Calorim* 2005, 79, 615.
20. Bassett, D. C.; Davitt, R. *Polymer* 1974, 15, 721.
21. Bassett, D. C.; Davitt, R. *Polymer* 1974, 15, 728.
22. Bunn, C. W.; Cobbold, A. J.; Palmer, R. P. *J Polym Sci* 1958, 28, 365.
23. Gall, M. J. *Polymer* 1974, 15, 272.
24. Briskman, B. A. *Nucl Instrum Meth B* 2007, 265, 276.
25. Lei, C.; Wang, X.; Fang, Q.; Gao, Y.; Tu, D.; Du, Q. *Eur Polym J* 2007, 43, 4523.
26. Khanna, Y. P. *J Mater Sci Lett* 1988, 7, 817.
27. Vandersanden, M. C. M.; Meijer, H. E. H. *Polymer* 1993, 34, 5063.
28. Araki, Y. *J Appl Polym Sci* 1965, 9, 3585.
29. Araki, Y. *J Appl Polym Sci* 1965, 9, 1515.
30. Koo, G. P.; Andrews, R. D. *Polym Eng Sci* 1969, 9, 268.
31. Durrell, W. S.; Stump, E. C.; Schuman, P. D. *J Polym Sci B: Polym Lett* 1965, 3, 831.
32. Araki, Y. *J Appl Polym Sci* 1967, 11, 953.
33. Noirez, L.; Baroni, P. *Appl Phys Lett* 2007, 24, 90.